Materials Innovations

HΣXA Publishers

Bio Materials | Research Article | http://doi.org/10.54738/MI.2021.1202

Synthesis of Biocompatible Fe_3O_4–TiO_2 Janus Nanocomposites for T_2 Magnetic Resonance Imaging and Photodynamic Therapy of Cancer In Vitro

Zhe Tang[1,2#], Yuguang Lu[1,2#], Yike Hou[1,2], Asim Mushtaq[1,2], Jabeen Farheen[1,2], Israt Ali[3], Saghir Hussain[4], M Zubair Iqbal[1,2*], Xiangdong Kong[1,2*]

1 Institute of Smart Biomedical Materials, School of Materials Science and Engineering, Zhejiang Sci-Tech University, 310018, Hangzhou, China
2 Zhejiang-Mauritius Joint Research Center for Biomaterials and Tissue Engineering, Zhejiang, China
3 Institute of Physics, Slovak Academy of Sciences, Dubravska Cesta 9,, Bratislava, 84511, Slovakia
4 Institute of Chemical Sciences, Bahauddin Zakariya University, Multan, 60000, Pakistan

Received: 12 December 2021
Accepted: 28 December 2021
Published: 31 December 2021

Citation: Tang Z, Lu Y, Hou Y, Mushtaq A, Farheen J, Ali I, Hussain S, Zubair Iqbal M, Kong X (2021) Synthesis of Biocompatible Fe_3O_4–TiO_2 Janus Nanocomposites for T_2 Magnetic Resonance Imaging and Photodynamic Therapy of Cancer In Vitro. Materials Innovations 1(2): 2-11.

***Correspondences**: (M Zubair Iqbal) zubair@zstu.edu.cn
(Xiangdong Kong) kongxd@zstu.edu.cn
# These authors contributed equally

Published By Hexa Publishers

ISSN
Electronic: 2790-1963

Janus nanoparticles are attaining profound interest due to their exciting and multifunctional properties generated from their asymmetric structures. However, control over synthesis, especially in solutions with small sizes, is a challenging concern. Herein, a simple hydrothermal method was applied to integrate the two highly biocompatible materials to design a Fe_3O_4-TiO_2 Janus structure. The structural characterization techniques were justified the asymmetric nature of the prepared nanocomposites. The average size of the JNPs was ~30 ± 2 nm, whereas the hydrodynamic size of Pluronic® F-127-coated JNPs was ~120 nm. The PF-127 modified Fe_3O_4-TiO_2 JNPs showed good biocompatibility, cancer cell targeting, and reactive oxygen species (ROS) generation ability. The designed nanocomposites yielded excellent r_2 relaxivity 18.2 $mM^{-1}s^{-1}$ and MR-image enchantment, suggesting their capability as a T_2-weighted contrast agent. Moreover, the PF127@Fe_3O_4-TiO_2 JNCs probe caused efficient photo-toxicity efficiency in vitro on 4T1 breast cancer cells under low-intensity UV light without any adverse effects to the control group. The present research provides a simple synthesis method and possesses an excellent imaging-guided therapeutic platform for future cancer treatment and biomedical applications.

Keywords: MRI Contrast Agents, Magnetic Nanocomposites, Janus Nanostructure, Hybrid Nanocomposites, Photodynamic Therapy

INTRODUCTION

Excellent progress has been made in materials science and technology during the recent few years. Notably, the synthesis of nanostructured materials with controllable size and shape has become an indispensable issue in nano-world[1]. The morphology and dimension of a nanoparticle are the most essential factors to alter the chemical and physical properties [2]. Therefore,

researchers have been paying attention to the controlled fabrication of nanomaterials with various shapes [3]. It is expected that changing the exterior morphology shape and dimensions of nanomaterials would award them with distinctive properties [4]. Recently, inorganic nanocomposite materials have attracted enormous interest in life and science[5]. To date, several techniques have been employed to synthesize various types of nanocomposites, such as matric-dispersed, core-shell, and Janus colloidal nanoparticles [6−9]. Among them, Janus nanoparticles (JNPs) have been attracted considerable attention owing to their novel anisotropic structure, multifunctional entities, and diverse potential applications ranging from science to medical [10,11]. However, the control synthesis of small and biocompatible Janus colloidal particles in solution remains a big challenge. Previously, various methods have been used to synthesize the JNPs, such as vapor deposition, electrostatic deposition, gel trapping technique, biphasic electrified jetting, masking, sputtering, and Pickering emulsion method [12]. However, implementing the techniques mentioned above requires sophisticated equipment, complex procedures, and rigorous experimental conditions. Therefore, developing a facile synthesis method to prepare JNPs is highly desired [13,14].

Recently, cancer diagnosis and treatment have been improved by nanotechnology, and nanoparticles offer significant hope to destroy cancerous cells because of their small size and surface functionalities for drug delivery systems. In cancer diagnosis, several techniques have been utilized to analyze melanoma, for example, X-ray, computed tomography (CT), magnetic resonance imaging (MRI), and positron emission tomography (PET) [15]. MRI is a non-invasive diagnosis modality with excellent safety, selectivity, and tissue categorization potential, and it does not produce high-ionization radiation that can aberrant DNA, which is generally exhibited during CT scans[16]. MRI often requires external contrast enchantment agents for improved visibility and precise diagnosis in early cancer detection and become a necessary part of MRI [17,18]. In clinics, 35% of MR scans were performed by gadolinium-based contrast agents. However, some severe drawbacks, including nephrogenic systemic fibrosis (NSF) and brain deposition, are associated with GBCAs, and researchers have been paying considerable attention to investigating the cause of gadolinium toxicity and new types of biocompatible contrast agents [1920]. Nowadays, manganese-based contrast agents are top-rated, and mangafodipir trisodium (Mn-DPDP) is absorbed by hepatocytes because of its chemical resemblance with vitamin B_6.

Nevertheless, the potential toxicity concerns are also ascribed with free Mn ions, which lead to developing the parkinsonism-like syndrome. These paramagnetic agents (Mn, Gd) have a considerably lower magnetic moment than super-paramagnetic agents [21]. Therefore, in addition to the development of contrast agents, iron oxide-based contrast agents have gained significant potential for positive and negative contrast enhancement. Superparamagnetic iron oxide nanoparticles (SPIONPs) are better substituting Gd and Mn-based contrast agents due to superior magnetic properties, high relaxation time, and good biocompatibility [22−24]. Compared with paramagnetic ions, a small dose of SPIONPs is administrated into the human body to conduct high-quality MRI.

In order to achieve remarkable therapeutic outcomes, imaging modalities are integrated with therapy functions to design theranostic agents [25]. The conventional cancer treatment options are surgery, radiotherapy, chemotherapy, and presently small molecule-based therapies are being adopted [26]. However, these kinds of therapies possessed severe side effects such as chemotherapy lefts systemic side effects, surgical resection of tumors retain high recurrence rate, and radiotherapy is also dependent on the radiation dose [27−29]. Therefore, modernization in the conventional tumor therapeutic techniques is very imperative. Moreover, researchers have also been paying attention to designing novel alternate treatment methods which are safe, positive, and cost-effective. Photodynamic therapy (PDT) is an alternative therapeutic methodology that utilizes a photosensitizer (PS), a suitable excitation light source, and oxygen molecules for treatment [30]. The ancient organic PDT agents, for example, Ce6 and ZnPc PS present easy light bleaching, quick circulation, low biostability, and poor water solubility [31].On the other hand, TiO_2, inorganic PS, has been considered a prospective photosensitizing mediator for PDT [32]. Titanium dioxide can activate under UV light to produce reactive oxygen species (ROS) to execute cancer cells. Various metallic nanoparticles have been doped into TiO_2 to obtained multifunctional applications such as imaging-guided phototherapy and sono-dynamic therapy of cancers. TiO_2 NPs have been investigated intensively using theoretical and experimental approaches due to their low cost, high photocatalytic properties, exceptional biocompatibility, physiological inertness, and high chemical strength [33].

In this report, a facile synthesis approach was adopted to fabricate the nanocompistes of TiO_2 and Fe_3O_4, two highly biocompatible nanoparticles which are suitable for preparation of Janus-shaped structure for enhanced T_2-MR-Imaging and photodynamic therapy of cancers (Schematic 1). Janus component material (TiO_2) was mixed under the solvothermal process, and then secondary particles Fe_3O_4 were produced using the hydrothermal method. The cytotoxicity, cellular uptake, ROS generation, magnetic resonance imaging properties, and photodynamic therapy of prepared Fe_3O_4-TiO_2 JNCs are discussed in detail.

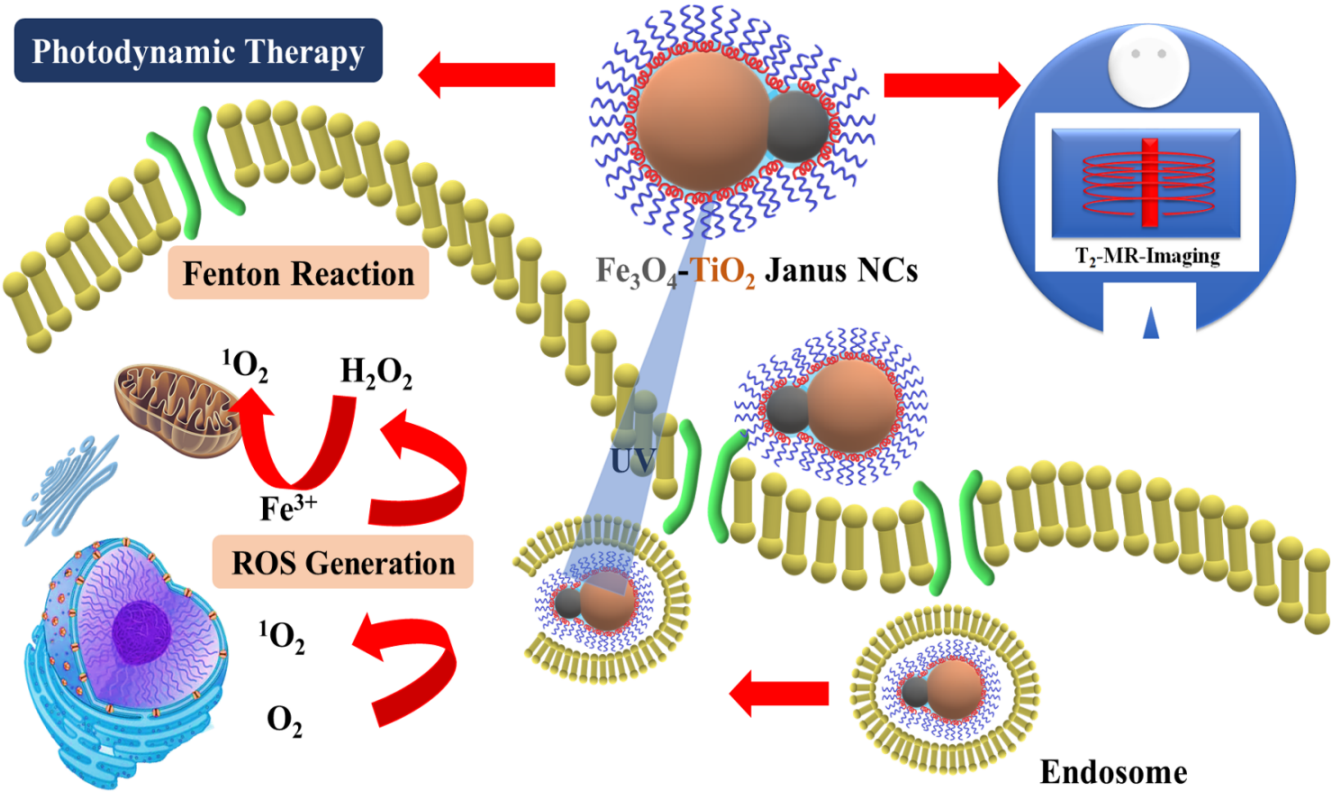

Scheme 1. The graphical representation of prepared Fe_3O_4-TiO_2 Janus nanocomposites for T_2-MR Imaging and Photodynamic therapy using ROS generation

EXPERIMENTAL SETUP

Synthesis of Fe_3O_4–TiO_2 Nanocomposites

The solvent-thermal method was adopted in the synthesis of monodisperse Fe_3O_4–TiO_2 nanocomposites. Briefly, TiO_2 nanoparticles with about 25 nm were fabricated based on the previously reported method and dispersed in toluene (10 mL) for further use[34]. In order to synthesize Fe_3O_4–TiO_2 nanocomposites, 150 mg of $Fe(acac)_3$ were dissolved in 4 mL of octadecane and 18 mL of n-octyl alcohol. Subsequently, TiO_2 (1 mL) was injected slowly into the above $Fe(acac)_3$ solution. The mixtures were being stirred for 4 h, the temperature was increased to 70 °C for 10 min to evaporate the non-polar solvent. Finally, the solution was cooled to room temperature and transferred into a Teflon-lined stainless steel autoclave. In the next step, the reaction temperature was kept at 240 °C for 2 h. Finally, the as-prepared Fe_3O_4–TiO_2 nanocomposites were washed by ethanol and centrifuged to collect the final product and dispersed in cyclohexane. Finally, Pluronic® F-127, FDA-approved triblock copolymer, was used to modify prepared materials to improve the biocompatibility and transfer the organic phase to aqueous. Briefly, PF127 (1 g) was dissolved well in trichloromethane $CHCl_3$ (100 mL), and then prepared Fe_3O_4-TiO_2 nanoparticles (1 mL) were added to the polymeric solution and stirred for 4 h. Next, water (10 mL) was added to the above solution to prepare an aqueous-organic emulsion. trichloromethane was removed using a rotary evaporator. Finally, aqueous dispersed nanocomposites were obtained and washed with ethanol before being dispersed in water (10 mL).

Characterization techniques

To acquire the structural and composition information of the as-prepared Fe_3O_4–TiO_2 nanocomposites, the Tecnai F20 transmission electron microscope (TEM) with Energy-dispersive X-ray spectroscopy (EDS) was used. Bruker AXS D8 X-Ray Diffractometer was used to investigate the crystal structure. The MR imaging and relaxivity performance of Fe_3O_4–TiO_2 nanocomposites were tested using MRI scanner system with a magnetic field of 0.55 T (Shanghai Niumag Corporation).

In Vitro Cytotoxicity of Fe_3O_4–TiO_2 JNCs

The toxicity behavior of prepared Fe_3O_4–TiO_2 nanocomposites was

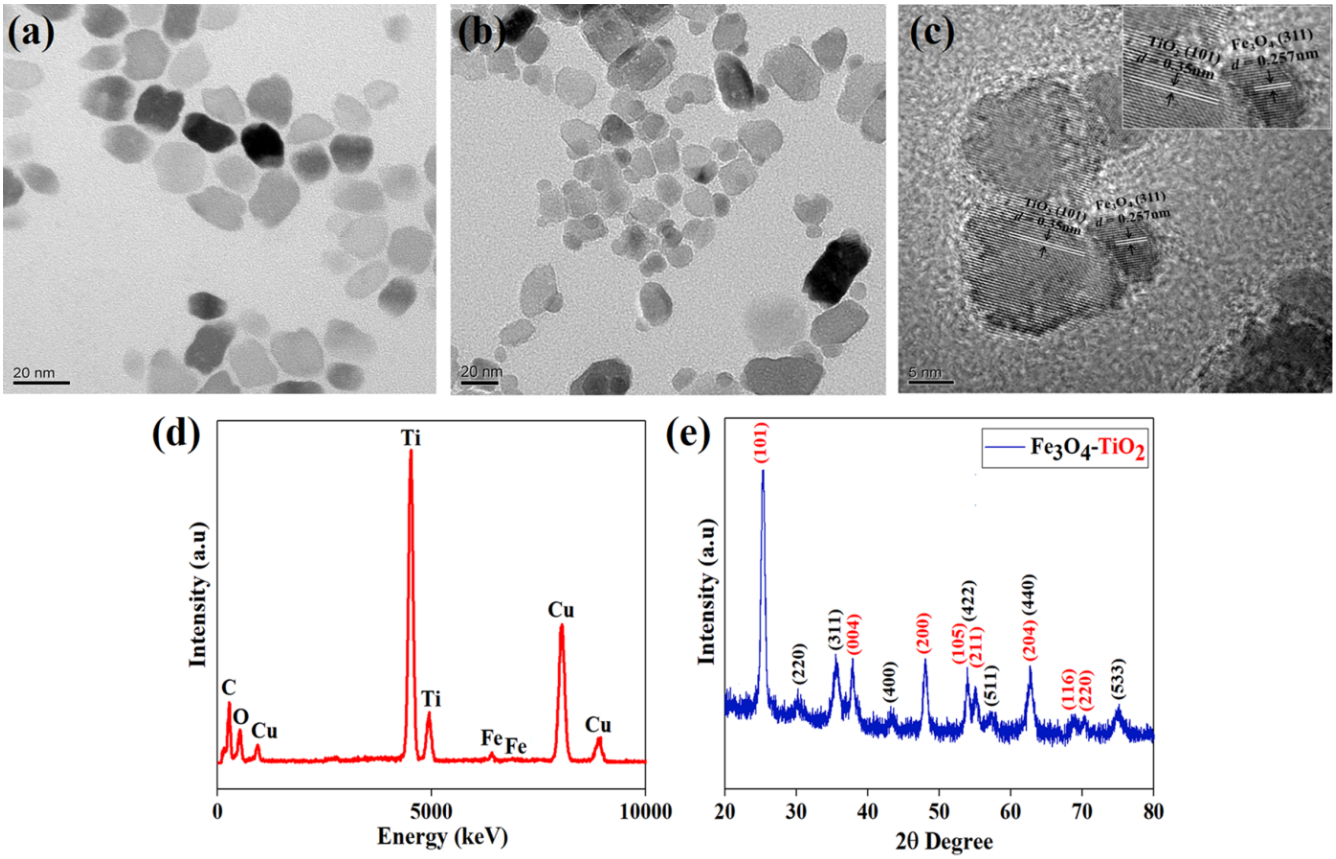

Figure 1. (a) TEM images of TiO_2 (b, c) TEM, HR-TEM images, (d) EDS spectra and (e) XRD spectra of prepared Fe_3O_4–TiO_2 nanocomposites.

examined through a colorimetric methyl thiazolyl tetrazolium (MTT) assay of 4T1 cells. Accordingly, 4T1 cells were seeded in a 96-well plate and then incubated with various concentrations of Fe_3O_4–TiO_2 nanocomposites (0, 10, 20, 40, 60, 80, and 100 μg mL^{-1}) for 24h, respectively. After that, the MTT assay was used to investigate the cell viability and pre/post-UV irradiation at different times. The power density of UV light was 6 mW cm^{-2} and incubated for 4 hours before checking viability. UV irradiation time was 0 min, 15 min, and 30 min. Finally, a microplate reader (iMark 168-1130, Bio-rad, USA) with a wavelength of 490 nm was used to evaluate the absorbance of each well.

Cellular uptake of Fe_3O_4-TiO_2 JNCs

For qualitative cellular uptake study was analyzed by confocal laser scanning microscopy (CLSM). 4T1 cells were seeded at a density of 3×10^5 cells in a petri dish in DMEM supplemented with 10 % FBS. The cells were allowed to attach to the plates for 12 h and then treated with Fe_3O_4-TiO_2 NCs for 6 h, where the NCs were labeled with fluorescein isothiocyanate (FITC). Then, the cells were rinsed with PBS three times and fixed with 4 % paraformaldehyde for 30 min. The cell membranes and nuclei were stained with DiI and DAPI, respectively, and the cells were observed by CLSM. For the qualitative assay, cytotoxicity was measured using the live/dead viability kit (Mesgen Biotech, Shanghai, China). Fe_3O_4-TiO_2 nanocomposites with different concentrations (0, 10 and 40 μg/mL) were co-cultured with the breast cancer 4T1 cells for 12 h. Then the culture substance was replaced with a fresh medium and exposed to UV light (6 $mW.cm^{-2}$) for 0, 15, and 30 min. After incubation for another 4 h at 37 °C, the cells were stained for 30 min with Calcein AM and propidium iodide (PI). Finally, the live/dead cells were detected using a confocal scanning laser microscope (A1, Nikon, Japan) with excitation and emission of green (Calcein-AM, ex/em = 488/518 nm) and red (PI, ex/em = 535/615 nm) fluorescence.

RESULTS AND DISCUSSION

The control over anisotropic growth is directly related to the hydrothermal temperature and reaction time. Experi-

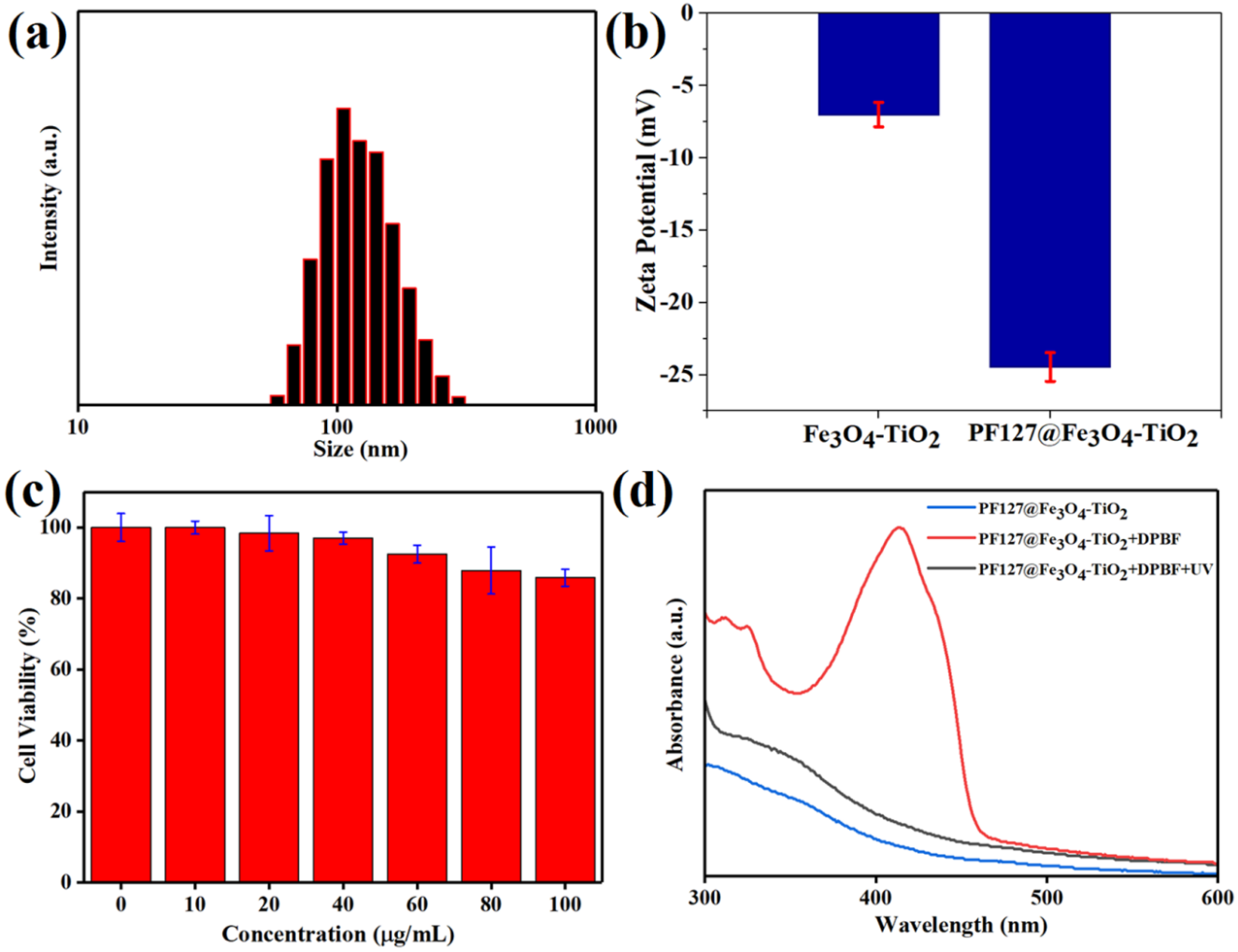

Figure 2. (a) Size histogram ofpolymer-coated nanocomposites using dynamic light scattering, (b) zeta potential of Fe_3O_4-TiO_2 and PF127 coated Fe_3O_4-TiO_2 nanocomposites, (c) toxicity evaluation profile using MTT assay using various concentrations of aqueous dispersed Janus nanocomposites, and (d) UV-vis absorbance spectrum of nanocomposites and ROS generation analysis.

mentally, two steps were carried out to synthesize Fe_3O_4-TiO_2 Janus-shaped nanocomposites. Firstly, seeds of TiO_2 nanoparticles were prepared using oleic acid and oleylamine (OM) by the decomposition of tetra-butyl titanate (TBOT). In the second step, Fe_3O_4 NPs were grown onto prepared TiO_2 at high temperature (220 °C) in the presence of organic surfactants, resulting in heterostructure or nanocomposites by the de-wetting process.

Before starting magnetic resonance imaging and photodynamic therapy of cancer, cellular uptake and cell-nanoparticle interaction information are important to examine. Figure 3 shows the laser confocal microscopy images of FITC loaded PF127@ Fe_3O_4-TiO_2 JNPs after incubation with 4T1 cells for 6 h. The fluorescent JNPs are noticeably penetrated into the cancerous cells, showing significant internalization, which is beneficial for therapeutics. Research showed that Pluronic F127 coating not only improves the biocompatibility of the nanoparticles but also possesses the complementary function to target the cancer cells without interaction with the normal cells. The good structural properties, biosafety, targeting ability, and ROS generation results of the synthesized JNPs certified their suitability for biomedical applications.

The successful preparation of TiO_2 NPs and Fe_3O_4-TiO_2 Janus-shaped structure was justified using TEM images (Figure 1). The well-dispersed TiO_2 NPs with an average size of 25±2 nm can be seen in Figure 1(a). The high magnification and high-resolution TEM images of prepared Fe_3O_4-TiO_2 JNCs are shown in Figure 1 (b, c), demonstrating that both materials are

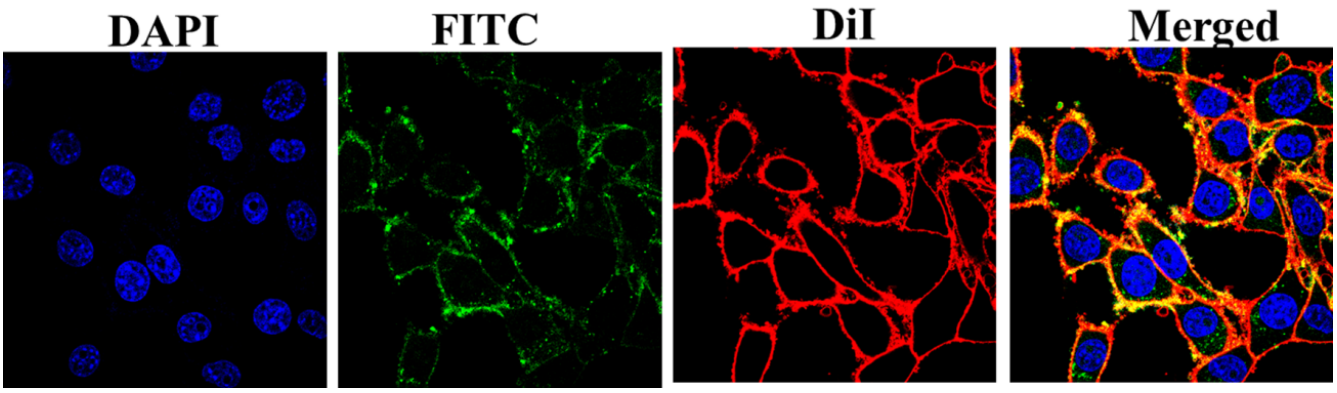

Figure 3. Cellular uptake investigation of FITClabeled PF127 coated Fe_3O_4-TiO_2 JNCs after incubation of 4T1 cancerous cells.

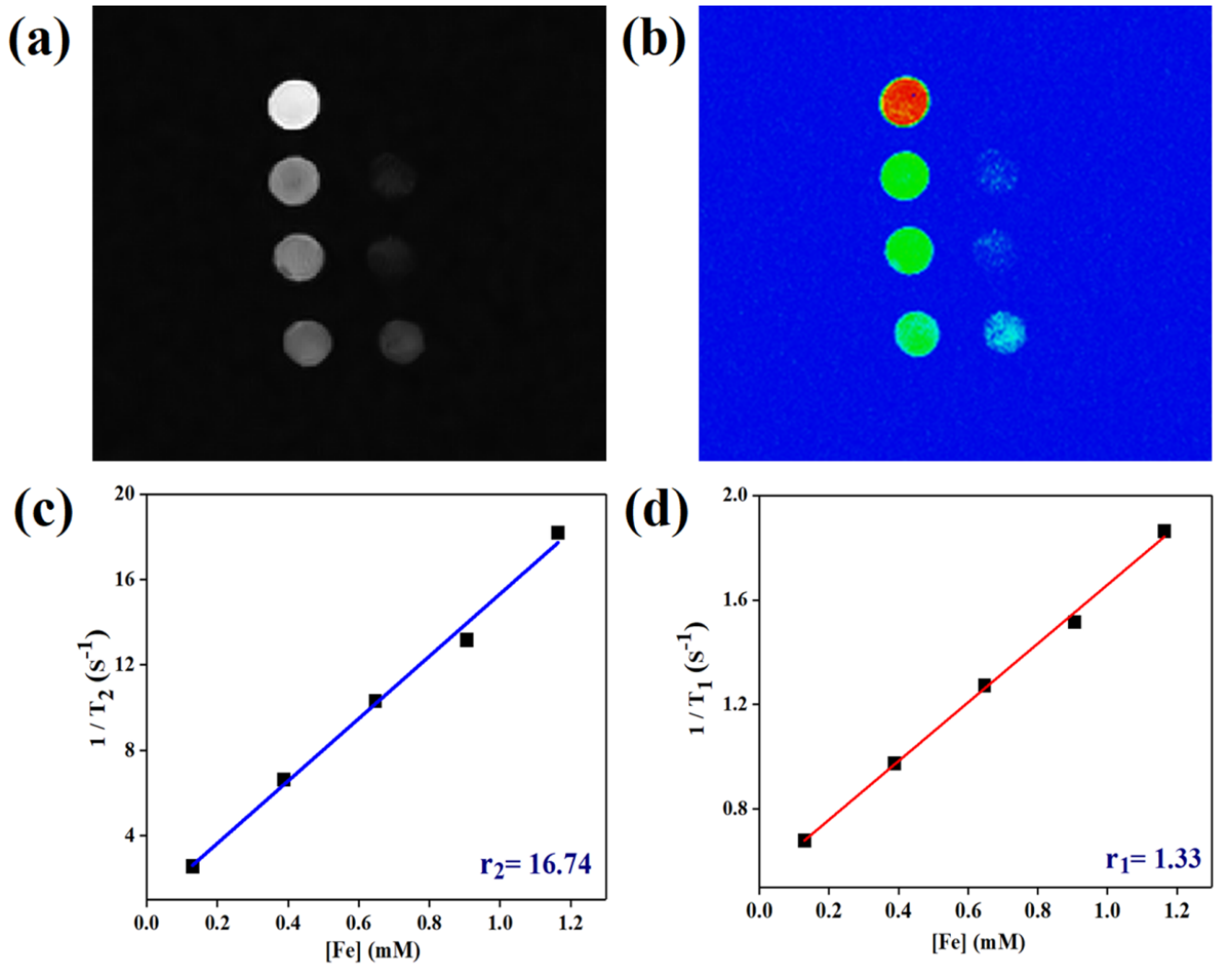

Figure 4. (a, b) T_2-weighted MR images and (c, d) a plot of r_2 and r_1 relaxivity values of the Fe_3O_4-TiO_2@PF-127 Janus nanostructure obtained using aqueous suspensions at various Fe concentrations.

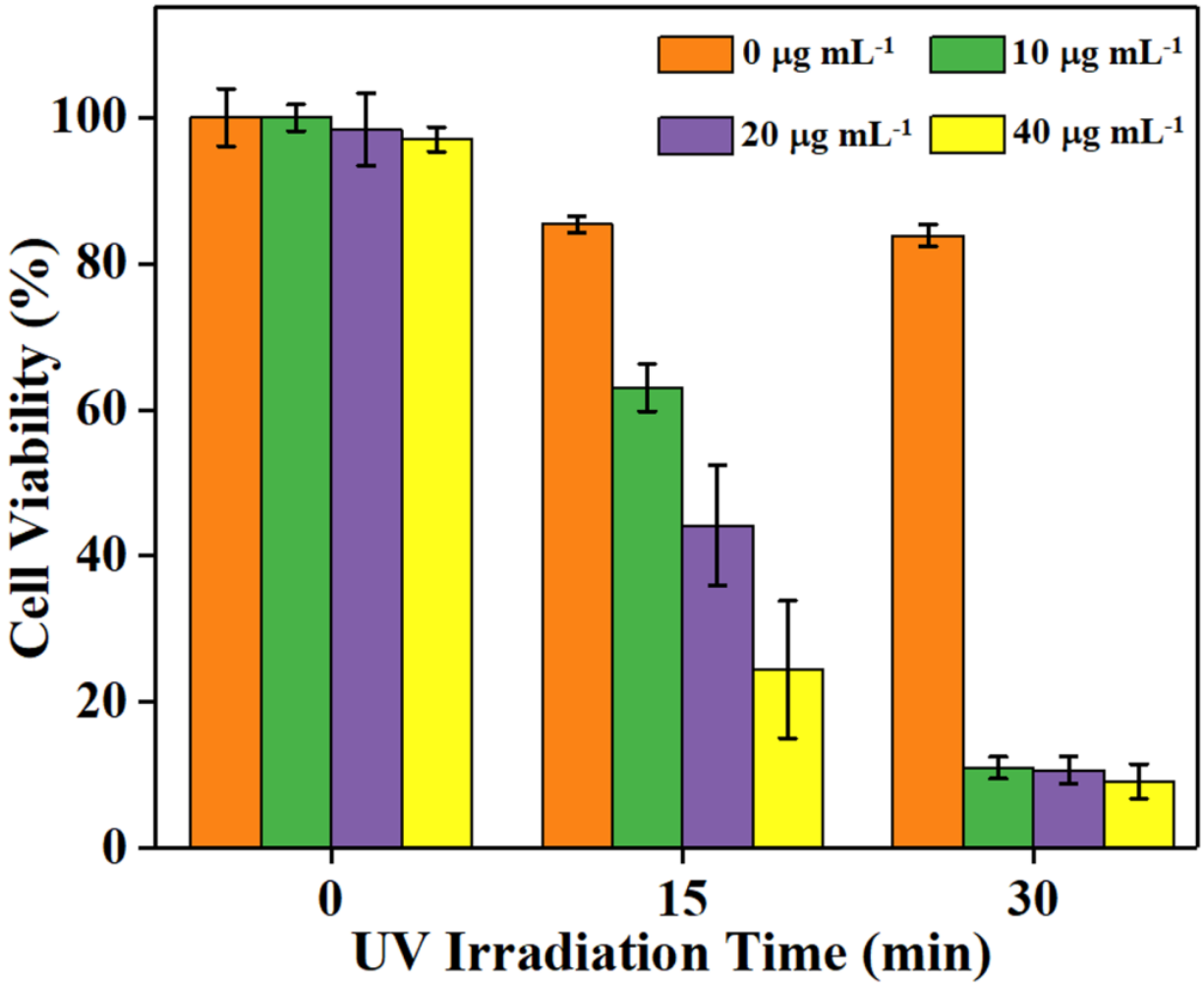

Figure 5. 4T1 breast cancer cell viability assessed after Fe_3O_4-TiO_2 nanocomposites were incubated with cells and UV light irradiation treatment at different times and concentrations

integrated in Janus shape with approximately 30±2 nm in sizes. HRTEM further noticeably illustrates the heterodimer pattern of prepared materials, and the inter-planar spacing 0.3517 nm and 0.2518 nm is well-matched with the (101) plane of TiO_2 and the (311) plane of Fe_3O_4, respectively. Furthermore, the EDS spectrum (Figure 1 d) also indicated the presence of Fe, Ti, and O elements, further providing evidence of the purity of prepared Fe_3O_4-TiO_2 nanocomposites.

The fabricated material was further investigated by X-ray powder diffraction to understand the crystal structure information. Figure 1(e) reveals the XRD spectra of Fe_3O_4-TiO_2 nanocomposites, demonstrating that the prepared material contains the peaks of both components. XRD spectra is well-matched with the tetragonal anatase structure of TiO_2 (JCPDS file No. 21-1272), and the tetragonal hausmannite structure of Fe_3O_4 (JCPDS file No. 24-0734). The overlap planes obviously show that the nature of the designed material is heterostructural. The structural results validate that the nanoparticles of Fe_3O_4 and TiO_2 are organized in Janus shape.

In order to improve the biocompatibility, FDA-approved triblock copolymer Pluronic F127 (PF127) was drafted onto the surface of JNCs. After coating, size and surface potential were assessed to identify the effect of surface modification which is critical for biomedical applications. The hydrodynamic size of the uncoated and PF127 coated JNPs was measured to be 70 nm and 150 nm, respectively. In addition, the zeta potential of the PF127 modified and unmodified JNPs was evaluated to be -24 eV and -8 eV, respectively. The good aqueous dispersion ability and zeta potential results indicate the suc-

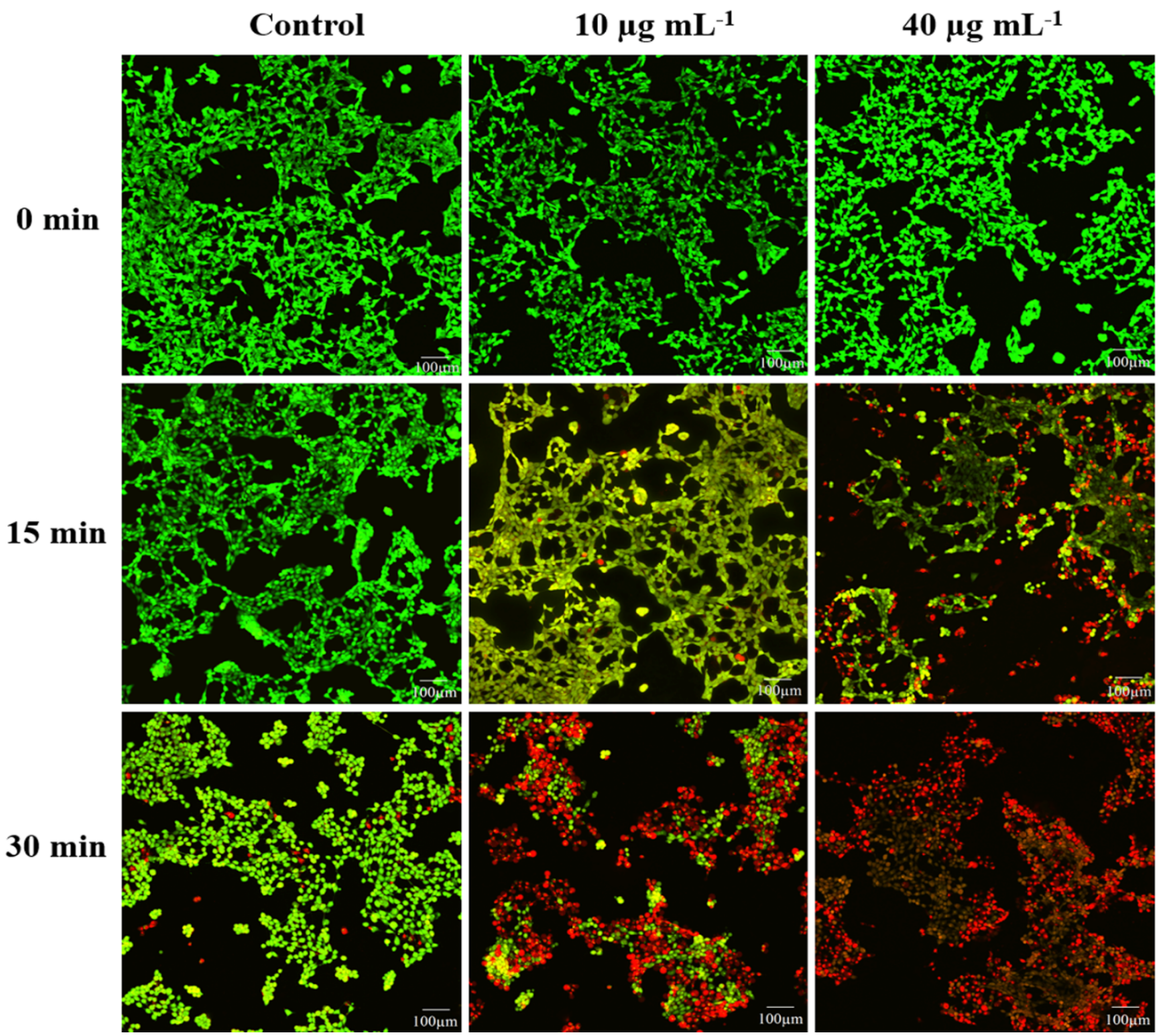

Figure 6. CLSM images of PI and Calcein-AM double-stained 4T1 cells under UV irradiation (scale bar is 100 µm).

cessful drafting for PF127 polymer. Cell cytotoxicity assessments of prepared JNPs were carried out by MTT assay using 4T1 mice breast cancer cell line. JNPs were incubated with the cancer cells, and over 90% cell survival rate (Figure 2c) was observed at a high concentration (100 μg mL^{-1}), showing promising biocompatibility of prepared Fe_3O_4-TiO_2 JNPs. Furthermore, UV-vis results showed that the Fe_3O_4 nanoparticles broaden the absorption from ultraviolet to visible region consistent with the previous reports [35]. After the improvement in the absorption, the increase in reactive oxygen species (ROS) must be carried out to understand the photo-killing efficiency of prepared JNCs. Therefore, 1,3-Diphenylisobenzofuran (DPBF), a common ROS quencher, was selected as a probe to examine the ROS level produced by Fe_3O_4-TiO_2 JNPs after UV treatment. DPBF responds irreversibly with ROS produced by photosensitizers, resulting in a decrease in absorption of the DPBF at 415 nm [36]. The JNCs combined with DPBF exhibited a noticeable absorption peak at 415 nm, corresponding to the DPBF. However, excellent degradation of DPBF is detected after the UV-irradiation (5 min), representing a high concentration of ROS generation (figure 2d) which induces apoptosis.

In order to take advantage of the magnetic (Fe_3O_4) component in the prepared nanocomposites, magnetic resonance imaging and relaxivity measurements were investigated using 0.55 T MRI scanner. The brightness of the phantom images decreased by increas-

ing the concentration of JNCs, demonstrating that the prepared sample has potency appreciably as a T_2- MRI contrast enhancement agent. The negative MR-Imaging signal strength is also distinct in color images (Figure 4 b). In addition, the calculated r_1 and r_2 value are about 1.1 $mM^{-1}S^{-1}$ and 18.2 $mM^{-1}S^{-1}$, respectively, further showing the suitability of JNPs as T_2 contrast agent.

The excellent biocompatibility and cellular uptake, photodynamic therapy (PDT) effect of the prepared Fe_3O_4-TiO_2 Janus NPs was tested against 4T1 cancer cells in the presence of an external UV irradiation source. The PDT efficacy was evaluated via MTT assay. Photo-toxicity mechanics are significantly based upon the exposure duration under UV irradiation and concentration of Fe_3O_4-TiO_2 JNPs as shown in Figure 5. It was observed that the viability of control groups (without JNCs and without UV irradiation) was not changed, indicating the dose safety of UV. Remarkably, maximum cells death was noticed in the JNCs groups under 30 min of UV irradiation with 6 mW cm^{-2}, resulting in the highest PDT efficacy of the synthesized Fe_3O_4-TiO_2 Janus NCs.

The CSLM images of 4T1 murine breast carcinoma cells further verified an in vitro efficiency of PDT. The green fluorescence emitted by live cells was prominently recorded from control groups, which revealed the nontoxic impact of UV irradiation at 6 mW cm^{-2} intensity over cancerous cells (Figure 6). While the significant increases in red fluorescence were observed as the exposure duration of UV irradiation and concentration of JNCs enhanced. The complete deceased of cancer cells were recorded at 40 μg mL^{-1} with 30 min of UV exposure supported the rationale of the maximum apoptosis rate. These results demonstrated that the prepared Fe_3O_4-TiO_2 Janus NCs extraordinarily generated in vitro reactive oxygen species such as singlet oxygen ($^1O_2$), as discussed above (Figure 2d), leading to effective carcinoma cells ablation under UV irradiation.

CONCLUSIONS

In this report, Fe_3O_4-TiO_2 anisotropic Janus nanoparticles are designed using a simple hydrothermal method. The secondary particle (Fe_3O_4) developed on the surface of the primary particle (TiO_2) to establish a Janus-shaped structure using the concept of epitaxial growth. The prepared JNCs showed homogeneous growth and admirable dispersion in non-polar solvents. Furthermore, the absorption of TiO_2 is shifted towards the visible region with the addition of Fe_3O_4. The PF127 coated nanocomposites revealed good biocompatibility and synergetic properties, resulting in enhanced cellular uptake and ROS generation. The designed JNCs demonstrated great T_2 contrast enchantment, which may help early diagnose liver cancer. Finally, the promising photodynamic therapeutic efficacy is achieved by Fe_3O_4-TiO_2 Janus nanocomposites, and mostly 4T1 breast cancer cells are died by the synergetic effect of the Janus structure under the low intensity of UV irradiation (6 mW cm^{-2}).

ACKNOWLEDGMENTS

The authors accept the funding from the National Natural Science Foundation of China (81950410638, 51672250), Key Research and Development Program of Zhejiang Province (2021C01180), Zhejiang Natural Science Foundation of China (LQ19E020010), and Zhejiang International Science and Technology Cooperation Project (2019C04020).

References

1) Jeevanandam, J.; Barhoum, A.; Chan, Y. S.; Dufresne, A.; Danquah, M. K. Review on nanoparticles and nanostructured materials: history, sources, toxicity and regulations. *Beilstein Journal of Nanotechnology* **2018**, *9*, 1050–1074, DOI: 10.3762/bjnano.9.98, available at https://dx.doi.org/10.3762/bjnano.9.98.
2) Patil, S. P.; Burungale, V. V. Physical and chemical properties of nanomaterials. *Nanomedicines for Breast Cancer Theranostics* **2020**, 17–31.
3) Gautam, P. K.; Singh, A.; Misra, K.; Sahoo, A. K.; Samanta, S. K. Synthesis and applications of biogenic nanomaterials in drinking and wastewater treatment. *Journal of Environmental Management* **2019**, *231*, 734–748, DOI: 10.1016/j.jenvman.2018.10.104, available at https://dx.doi.org/10.1016/j.jenvman.2018.10.104.
4) Saleh, T. A. Nanomaterials: Classification, properties, and environmental toxicities. *Environmental Technology & Innovation* **2020**, *20*, 101067–101067.
5) Rani, P.; Kasneryk, V.; Opanasenko, M. MOF-inorganic nanocomposites: Bridging a gap with inorganic materials. *Applied Materials Today* **2021**, 101283–101283, DOI: 10.1016/j.apmt.2021.101283, available at https://dx.doi.org/10.1016/j.apmt.2021.101283.
6) Mahmood, A.; Zou, R.; Wang, Q.; Xia, W.; Tabassum, H.; Qiu, B.; Zhao, R. Nanostructured Electrode Materials Derived from Metal–Organic Framework Xerogels for High-Energy-Density Asymmetric Supercapacitor. *ACS Applied Materials & Interfaces* **2016**, *8*, 2148–2157, DOI: 10.1021/acsami.5b10725, available at https://dx.doi.org/10.1021/acsami.5b10725.
7) Mahmood, A.; Wang, J.-L. A Review of Grazing Incidence Small- and Wide-Angle X-Ray Scattering Techniques for Exploring the Film Morphology of Organic Solar Cells. *Solar RRL* **2020**, *4*, 2000337–2000337, DOI: 10.1002/solr.202000337, available at https://dx.doi.org/10.1002/solr.202000337.
8) Mushtaq, A.; Hou, Y.; Tian, C.; Deng, T.; Xu, C.; Sun, Z.; Kong, X.; Iqbal, M. Z. Facile synthesis of Mn doped TiO2 rhombic nanocomposites for enhanced T1-Magnetic resonance imaging and photodynamic therapy. *Materials Research Bulletin* **2021**, *144*, 111481–111481, DOI: 10.1016/j.materresbull.2021.111481, available at https://dx.doi.org/10.1016/j.materresbull.2021.111481.
9) Zhao, R.; Cao, J.; Yang, X.; Zhang, Q.; Iqbal, M. Z.; Lu, J.; Kong, X. Inorganic material based macrophage regulation for cancer therapy: basic concepts and recent advances. *Biomaterials Science* **2021**, *2021*, 4568–4590, DOI: 10.1039/d1bm00508a, available at https://dx.doi.org/10.1039/d1bm00508a.
10) Zhang, X.; Fu, Q.; Duan, H.; Song, J.; Yang, H. Janus Nanoparticles: From Fabrication to (Bio)Applications. *ACS Nano* **2021**, *15*, 6147–6191, DOI: 10.1021/acsnano.1c01146, available at https://dx.doi.org/10.1021/acsnano.1c01146.

11) Safaie, N.; Ferrier, R. C. Janus nanoparticle synthesis: Overview, recent developments, and applications. *Journal of Applied Physics* **2020**, *127*, 170902–170902, DOI: 10.1063/5.0003329, available at https://dx.doi.org/10.1063/5.0003329.
12) Rahiminezhad, Z.; Tamaddon, A. M.; Borandeh, S.; Abolmaali, S. S. Janus nanoparticles: New generation of multifunctional nanocarriers in drug delivery, bioimaging and theranostics. *Applied Materials Today* **2020**, *18*, 100513–100513, DOI: 10.1016/j.apmt.2019.100513, available at https://dx.doi.org/10.1016/j.apmt.2019.100513.
13) Li, X.; Chen, L.; Cui, D.; Jiang, W.; Han, L.; Niu, N. Preparation and application of Janus nanoparticles: Recent development and prospects. *Coordination Chemistry Reviews* **2022**, *454*, 214318–214318, DOI: 10.1016/j.ccr.2021.214318, available at https://dx.doi.org/10.1016/j.ccr.2021.214318.
14) Dar, G. I.; Iqbal, M. Z.; AiguoWu, Multifunctional biocompatible Janus nanostructures for biomedical applications. *Current Opinion in Biomedical Engineering* **2019**, *10*, 79–88, DOI: 10.1016/j.cobme.2019.04.001, available at https://dx.doi.org/10.1016/j.cobme.2019.04.001.
15) Jafari, S. H.; Saadatpour, Z.; Salmaninejad, A.; Momeni, F.; Mokhtari, M.; Nahand, J. S.; Rahmati, M.; Mirzaei, H.; Kianmehr, M. Breast cancer diagnosis: Imaging techniques and biochemical markers. *Journal of Cellular Physiology* **2018**, *233*, 5200–5213, DOI: 10.1002/jcp.26379, available at https://dx.doi.org/10.1002/jcp.26379.
16) Nazarian, S.; Hansford, R.; Rahsepar, A. A.; Weltin, V.; McVeigh, D.; Ipek, E. G.; Kwan, A.; Berger, R. D.; Calkins, H.; Lardo, A. C.; Kraut, M. A.; Kamel, I. R.; Zimmerman, S. L.; Halperin, H. R. Safety of Magnetic Resonance Imaging in Patients with Cardiac Devices. *New England Journal of Medicine* **2017**, *377*, 2555–2564, DOI: 10.1056/nejmoa1604267, available at https://dx.doi.org/10.1056/nejmoa1604267.
17) Pan, C.; Lin, J.; Zheng, J.; Liu, C.; Yuan, B.; Akakuru, O. U.; Iqbal, M. Z.; Fang, Q.; Hu, J.; Chen, J.; Lin, J.; Dai, Q.; Guo, X.; Li, Z.; Zhang, T.; Xu, C.; Ma, X.; Chen, T.; Wu, A.; Jin, Y. An intelligent T1–T2 switchable MRI contrast agent for the non-invasive identification of vulnerable atherosclerotic plaques. *Nanoscale* **2021**, *13*, 6461–6474, DOI: 10.1039/d0nr08039j, available at https://dx.doi.org/10.1039/d0nr08039j.
18) Sammet, S. Magnetic resonance safety. *Abdominal Radiology* **2016**, *41*, 444–451, DOI: 10.1007/s00261-016-0680-4, available at https://dx.doi.org/10.1007/s00261-016-0680-4.
19) Mathur, M.; Jones, J. R.; Weinreb, J. C. Gadolinium Deposition and Nephrogenic Systemic Fibrosis: A Radiologist's Primer. *RadioGraphics* **2020**, *40*, 153–162, DOI: 10.1148/rg.2020190110, available at https://dx.doi.org/10.1148/rg.2020190110.
20) Kribben, A.; Witzke, O.; Hillen, U.; Barkhausen, J.; Daul, A. E.; Erbel, R. Nephrogenic Systemic Fibrosis: Pathogenesis, Diagnosis, and Therapy. *Journal of the American College of Cardiology* **2009**, *53*, 1621–1628.
21) Brito, B.; Price, T. W.; Gallo, J.; Bañobre-López, M.; Stasiuk, G. J. Smart magnetic resonance imaging-based theranostics for cancer. *Theranostics* **2021**, *11*, 8706–8737, DOI: 10.7150/thno.57004, available at https://dx.doi.org/10.7150/thno.57004.
22) Iqbal, M. Z.; Ma, X.; Chen, T.; Zhang, L.; Ren, W.; Xiang, L.; Wu, A. Silica-coated super-paramagnetic iron oxide nanoparticles (SPIONPs): a new type contrast agent of T1 magnetic resonance imaging (MRI). *Journal of Materials Chemistry B* **2015**, *3*, 5172–5181, DOI: 10.1039/c5tb00300h, available at https://dx.doi.org/10.1039/c5tb00300h.
23) Israel, L. L.; Galstyan, A.; Holler, E.; Ljubimova, J. Y. Magnetic iron oxide nanoparticles for imaging, targeting and treatment of primary and metastatic tumors of the brain. *Journal of Controlled Release* **2020**, *320*, 45–62, DOI: 10.1016/j.jconrel.2020.01.009, available at https://dx.doi.org/10.1016/j.jconrel.2020.01.009.
24) Javed, Y.; Akhtar, K.; Anwar, H.; Jamil, Y. MRI based on iron oxide nanoparticles contrast agents: effect of oxidation state and architecture. *Journal of Nanoparticle Research* **2017**, *19*, 366–366, DOI: 10.1007/s11051-017-4045-x, available at https://dx.doi.org/10.1007/s11051-017-4045-x.
25) Iqbal, M. Z.; Ali, I.; Khan, W. S.; Kong, X.; Dempsey, E. Reversible self-assembly of gold nanoparticles in response to external stimuli. *Materials & Design* **2021**, *205*, 109694–109694, DOI: 10.1016/j.matdes.2021.109694, available at https://dx.doi.org/10.1016/j.matdes.2021.109694.
26) Pearce, A.; Haas, M.; Viney, R.; Pearson, S.-A.; Haywood, P.; Brown, C.; Ward, R. Incidence and severity of self-reported chemotherapy side effects in routine care: A prospective cohort study. *PLOS ONE* **2017**, *12*, e0184360–e0184360, DOI: 10.1371/journal.pone.0184360, available at https://dx.doi.org/10.1371/journal.pone.0184360.
27) Schirrmacher, V. From chemotherapy to biological therapy: A review of novel concepts to reduce the side effects of systemic cancer treatment (Review). *International Journal of Oncology* **2019**, *54*, 407–419.
28) Oun, R.; Moussa, Y. E.; Wheate, N. J. The side effects of platinum-based chemotherapy drugs: a review for chemists. *Dalton Transactions* **2018**, *47*, 6645–6653, DOI: 10.1039/c8dt00838h, available at https://dx.doi.org/10.1039/c8dt00838h.
29) Qi, X.; Wang, Z.; Yang, X.; Wang, J.; Wang, S.; Mao, X.; Li, M.; Zhao, Y.; Wang, W.; Wu, T. Risk of serious adverse event and fatal adverse event with molecular target anticancer drugs in cancer patients: A meta-analysis. *Journal of Cancer Research and Therapeutics* **2019**, *15*, 1435–1435, DOI: 10.4103/jcrt.jcrt_577_18, available at https://dx.doi.org/10.4103/jcrt.jcrt_577_18.
30) Hu, D.; Sheng, Z.; Gao, G.; Siu, F.; Liu, C.; Wan, Q.; Gong, P.; Zheng, H.; Ma, Y.; Cai, L. Activatable albumin-photosensitizer nanoassemblies for triple-modal imaging and thermal-modulated photodynamic therapy of cancer. *Biomaterials* **2016**, *93*, 10–19, DOI: 10.1016/j.biomaterials.2016.03.037, available at https://dx.doi.org/10.1016/j.biomaterials.2016.03.037.
31) Hong, S. H.; Koo, M.-A.; Lee, M. H.; Seon, G. M.; Park, Y. J.; Jeong, H.; Kim, D.; Park, J.-C. An effective method to generate controllable levels of ROS for the enhancement of HUVEC proliferation using a chlorin e6-immobilized PET film as a photo-functional biomaterial. *Regenerative Biomaterials* **2021**, *8*, DOI: 10.1093/rb/rbab005, available at https://dx.doi.org/10.1093/rb/rbab005.
32) Li, J.; Wang, X.; Jiang, H.; Lu, X.; Zhu, Y.; Chen, B. New strategy of photodynamic treatment of TiO2 nanofibers combined with celastrol for HepG2 proliferation in vitro. *Nanoscale* **2011**, *3*, 3115–3115, DOI: 10.1039/c1nr10185d, available at https://dx.doi.org/10.1039/c1nr10185d.
33) Zhang, S.; Yang, D.; Jing, D.; Liu, H.; Liu, L.; Jia, Y.; Gao, M.; Guo, L.; Huo, Z. Enhanced photodynamic therapy of mixed phase TiO2(B)/anatase nanofibers for killing of HeLa cells. *Nano Research* **2014**, *7*, 1659–1669, DOI: 10.1007/s12274-014-0526-8, available at https://dx.doi.org/10.1007/s12274-014-0526-8.
34) Iqbal, M. Z.; Ren, W.; Saeed, M.; Chen, T.; Ma, X.; Yu, X.; Zhang, J.; Zhang, L.; Li, A.; Wu, A. A facile fabrication route for binary transition metal oxide-based Janus nanoparticles for cancer theranostic applications. *Nano Research* **2018**, *11*, 5735–5750, DOI: 10.1007/s12274-017-1628-x, available at https://dx.doi.org/10.1007/s12274-017-1628-x.
35) Wardiayati, S.; Dewi, S. H. Influence of Fe3O4 Addition in TiO2 Catalyst on The Degradation Process of Methylene Blue. *Journal of Physics: Conference Series* **2018**, *1091*, 012015–012015, DOI: 10.1088/1742-6596/1091/1/012015, available at https://dx.doi.org/10.1088/1742-6596/1091/1/012015.
36) Nsubuga, A.; Mandl, G. A.; Capobianco, J. A. Investigating the reactive oxygen species production of Rose Bengal and Merocyanine 540-loaded radioluminescent nanoparticles. *Nanoscale Advances* **2021**, *3*, 1375–1381, DOI: 10.1039/d0na00964d, available at https://dx.doi.org/10.1039/d0na00964d.